

Article

# Improving Thermal Stability of Polyurethane through the Addition of Hyperbranched Polysiloxane

Shang-Hao Liu <sup>1</sup>, Ming-Yuan Shen <sup>2</sup>, Chen-Feng Kuan <sup>3</sup>, Hsu-Chiang Kuan <sup>3</sup> , Cing-Yu Ke <sup>4</sup> and Chin-Lung Chiang <sup>4,\*</sup> 

<sup>1</sup> Department of Ammunition Engineering and Explosion Technology, Anhui University of Science and Technology, Huainan 232001, Anhui, China; u9414042@cmu.edu.tw

<sup>2</sup> Department of Mechanical Engineering, National Chin-Yi University of Technology, Taichung 411, Taiwan; hbj678@gmail.com

<sup>3</sup> Department of Food Beverage Management, Far East University, Tainan 744, Taiwan; cfkuan@mail.feue.edu.tw (C.-F.K.); hckuan@mail.feue.edu.tw (H.-C.K.)

<sup>4</sup> Green Flame Retardant Material Research Laboratory, Department of Safety, Health and Environmental Engineering, Hung-Kuang University, Taichung 433, Taiwan; n74731@gmail.com

\* Correspondence: dragon@sunrise.hk.edu.tw; Tel.: +886-4-2631-8652-4008

Received: 1 March 2019; Accepted: 11 April 2019; Published: 16 April 2019



**Abstract:** Polydimethylsiloxane with hydroxy groups was functionalized to form functionalized polydimethylsiloxane, which subsequently underwent an addition reaction with isophorone diisocyanate to form the prepolymer. Next, 3-aminopropyltriethoxysilane (APTS) reacted with 3-glycidoxypropyltrimethoxysilane (GPTS) to produce bridged polysilsesquioxanes, and sol-gel technology was employed to form hyperbranched polysiloxane nanoparticles with hydroxy groups, APTS-GPTS, which was used as the additive. The hyperbranched polysiloxane and the prepolymer containing NCO functional groups then underwent an addition reaction to produce the hybrid materials. Fourier-transform infrared spectroscopy and <sup>29</sup>Si nuclear magnetic resonance were used to characterize the structure of the polyurethane hybrid. Regarding thermal stability, after the hyperbranched polysiloxane nanoparticles was introduced, the integral procedural decomposition temperature increased from 348 °C for polyurethane matrix to 859 °C for the hybrid material. The results reveal that the thermal stability of the hybrid material substantially increased by approximately 247%.

**Keywords:** polyurethane (PU), siloxane; sol-gel technology; thermogravimetric analysis; thermal stability

## 1. Introduction

Polyurethane (PU) is a common high-performance polymer that features favorable mechanical properties, chemical resistance, and wear resistance. Polyurethane material is widely applied in automobile manufacturing, the textile industry, sporting equipment, shoe soles, and coating materials [1,2]. Despite its versatility, PU is not resistant to heat. For example, the mechanical properties of PU deteriorate rapidly when the temperature reaches 90 °C or higher. Furthermore, PU undergoes severe pyrolysis when the temperature exceeds 200 °C. Therefore, limiting applications of PU is critical to the development of polymer materials [3–5].

Numerous studies have investigated the siloxane structure, which is unique in terms of its thermal stability, hydrophobicity, weatherability, high gas penetrability, low toxicity, insulative properties, and excellent ultraviolet resistance. This structure can effectively enhance the heat resistance of polymer materials that have been mixed with siloxane, thereby expanding the application scope of polymer materials [6–8].

PU possesses excellent properties but has limited applications because it has poor thermal stability and easily combusts. By comparison, the main chain of siloxane is the Si-O bond, which has high bond energy and significant chain flexibility; thus, siloxane features superior thermal stability under high temperature [9,10]. In this study, the sol-gel technology was adopted to mix organic and inorganic materials to form a siloxane-PU hybrid material. Subsequently, Fourier-transform infrared spectroscopy (FTIR) was employed to identify the structure of the hybrid material, and solid-state  $^{29}\text{Si}$  nuclear magnetic resonance (NMR) spectroscopy was used to identify the condensation density of the Si-PU/APTS-GPTS hybrid material. The thermal stability and heat resistance of the developed hybrid materials were examined using thermogravimetric analysis (TGA) and the integral procedural decomposition temperature (IPDT).

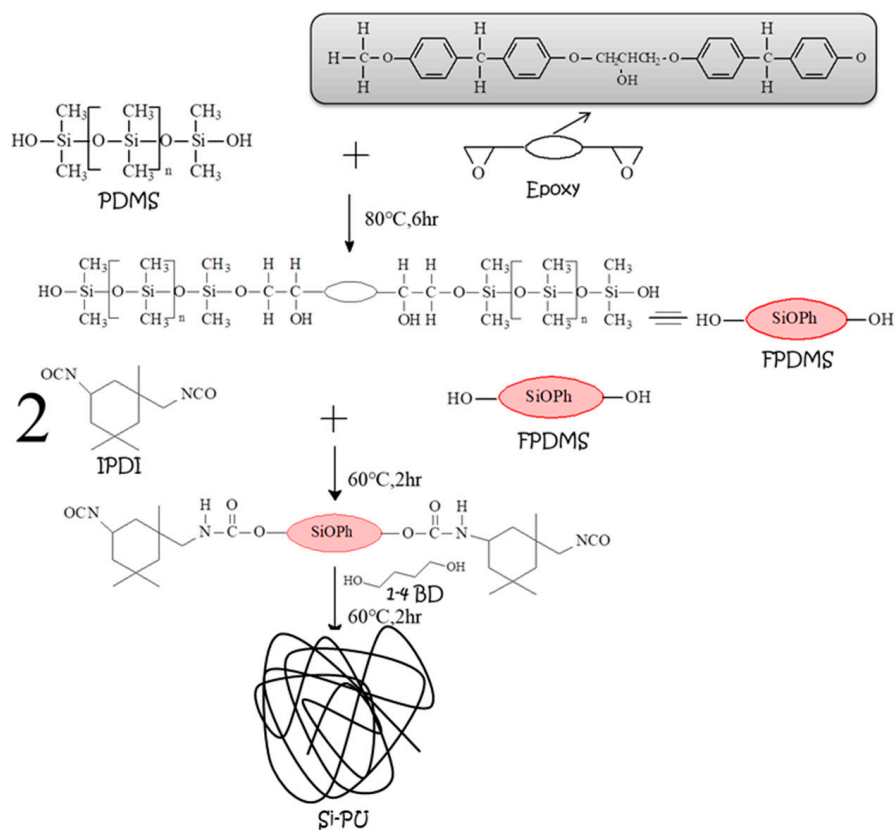
## 2. Experiment

### 2.1. Materials

Diglycidyl ether of bisphenol A (DGEBA) with an epoxide equivalent weight (EEW) of  $180 \text{ g eq}^{-1}$  was obtained from Nan-Ya Plastics Corporation, Taipei, Taiwan. Diaminodiphenylmethane (DDM), which was used as curing agent for epoxy resin, was purchased from TCI Chemical Co, Tokyo, Japan. *N,N*-Dimethylbenzylamine (NDBA), 1,4-butanediol(1,4-BD), 3-aminopropyltriethoxysilane (APTS) and 3-glycidoxypropyltrimethoxysilane (GPTS) were purchased from Acros Chemical Co, Springfield Township, NJ, USA. Polydimethylsiloxane KF-6000 (PDMS) was purchased from Topco Technologies Corp, Taipei, Taiwan. Anhydrous stabilized tetrahydrofuran (THF) was obtained from Lancaster Co., Morecambe, Lancashire, UK. Isophorone diisocyanate (IPDI) and dibutyltin dilaurate (DBTDL) were purchased from Alfa Aesar CO., Shore Road, Heysham, LA3 2XY, UK. Hydrogen chloride (HCl) was purchased from ECHO Chemical Co., LTD, Toufen Chen, Miaoli, Taiwan.

### 2.2. Preparation of Si-PU

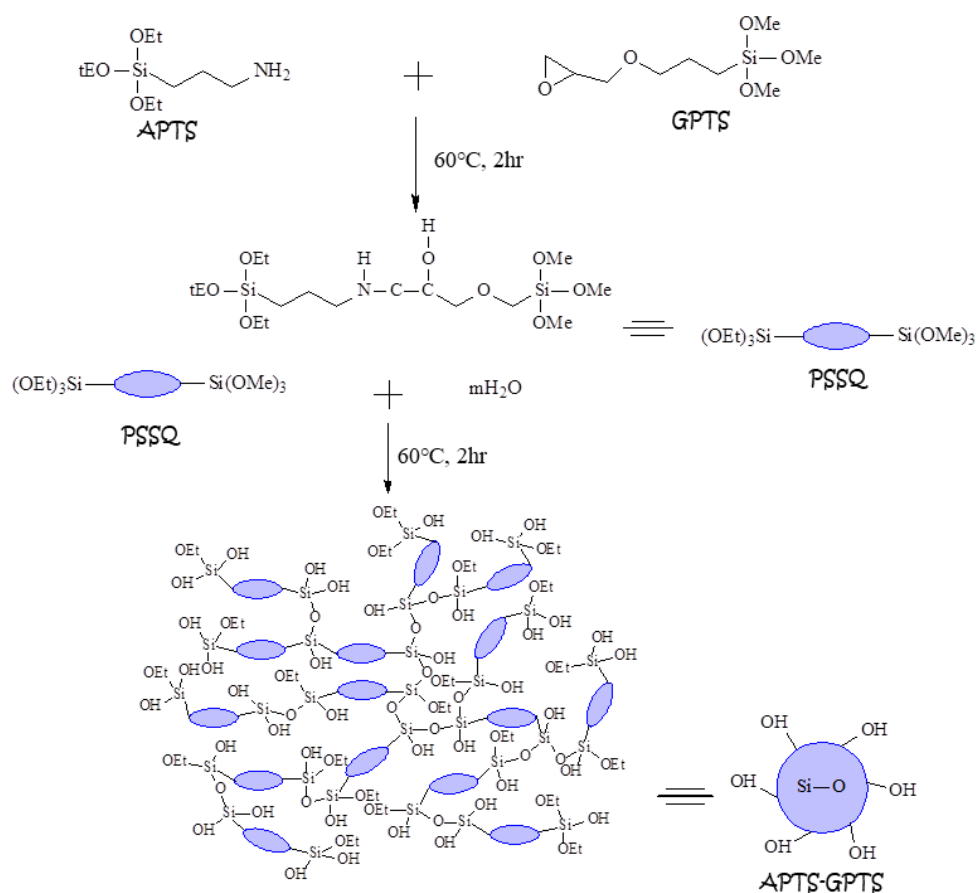
PDMS (18.24 g) with hydroxy groups (-OH) and epoxy (1.76 g) were placed in a 100-mL serum vial and underwent magnetic and mechanical agitation in a nitrogen environment at  $80 \text{ }^\circ\text{C}$ . NDBA catalyst (0.2 g) was then added to the serum vial to react with the mixture for 6 h to form the functionalized polydimethylsiloxane (FPDMS). After the temperature was reduced to  $40 \text{ }^\circ\text{C}$ , 8.88 g of IPDI and 20 g of FPDMS were placed in a four-neck flask in nitrogen environment and then underwent magnetic and mechanical agitation at  $80 \text{ }^\circ\text{C}$ . Subsequently, DBTDL catalyst (0.3 g) was added to the four-neck flask to react, forming a prepolymer. After reacting for 2 h, the viscosity of the prepolymer was increased to a degree similar to that of maltose, and subsequently added 80 mL of THF solvent and 0.8 g of 1,4-butanediol chain extender to react for 1 h to form polyurethane containing silicon, Si-PU. After the viscosity increased, Si-PU was placed into to a Teflon mold. The mold was first placed in a vacuum oven for deaeration at  $80 \text{ }^\circ\text{C}$  for 24 h and then placed in a circulating oven for 24 h at  $80 \text{ }^\circ\text{C}$ . The finished product was then removed from the mold and placed at room temperature to cool, and completed the preparation of Si-PU. The reaction of Si-PU is presented in Scheme 1.



Scheme 1. The reaction of Si-PU.

### 2.3. Preparation of APTS-GPTS

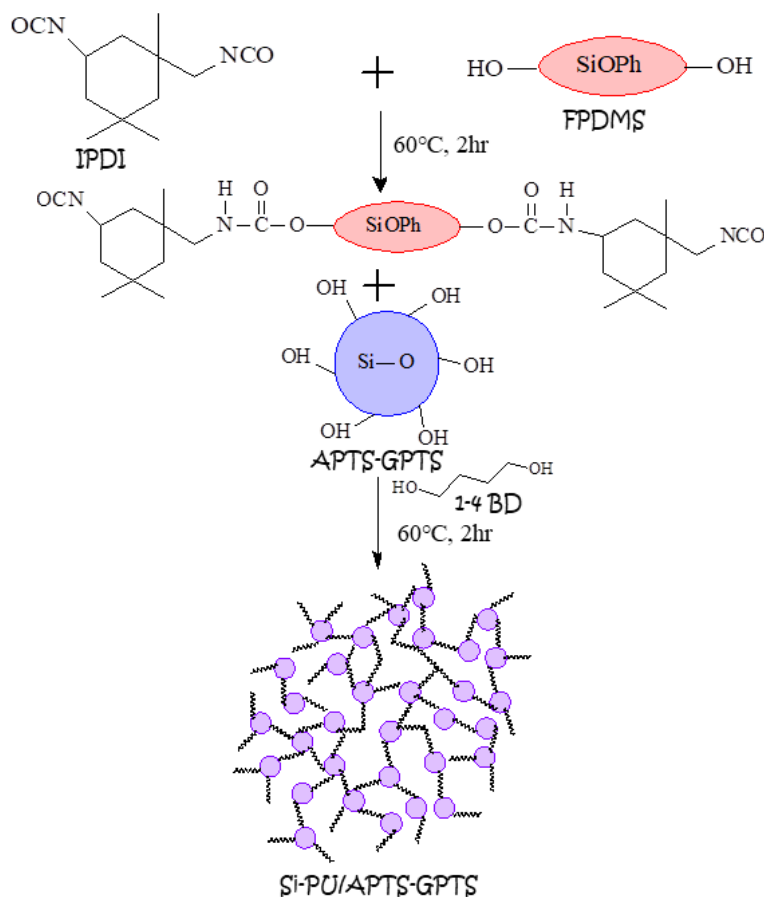
APTS (1.55 g) and GPTS (1.65 g) were added to a 100-mL serum vial with 80 mL of THF solvent for agitation; after reacting for 2 h, Solution A was obtained. Next, the THF solvent was added to 0.72 mL of deionized water and hydrogen chloride was instilled, and the pH value was adjusted to 4, thereby obtaining Solution B. Finally, Solution B was slowly instilled into Solution A and underwent a sol-gel reaction for 2 h at 60 °C to obtain APTS-GPTS, the reaction of which is shown in Scheme 2.



**Scheme 2.** The reaction of APTS-GPTS.

#### 2.4. Preparation of Si-PU/APTS-GPTS

Prepolymer (28.88 g) was added to 80 mL of THF solvent and APTS-GPTS (19.8 g) was slowly instilled and left for 2 h to react to observe whether the viscosity had increased and the fluid level had decreased. After the viscosity had increased, the mixture was poured into a Teflon mold. The mold was first placed in the vacuum oven for deaeration for 24 h. Once the temperature was 80 °C, it was then placed in the cyclic oven for 24 h. Once the temperature had reached 80 °C, the finished product was then removed from the mold and cooled to room temperature, thereby completing the preparation of Si-PU/APTS-GPTS. The reaction of Si-PU/APTS-GPTS is shown in Scheme 3.



**Scheme 3.** The reaction of Si-PU/APTS-GPTS.

## 2.5. Measurements

The FTIR spectra of the materials were recorded within 4000–400  $\text{cm}^{-1}$  using a Nicolet Avatar 320 FT-IR spectrometer, from Analytical Instruments Brokers LLC, Golden Valley, MN, USA. Thin films were prepared by the solution-casting method. A minimum of 32 scans were signal-averaged with a resolution of 2  $\text{cm}^{-1}$  in the 4000–400  $\text{cm}^{-1}$  range.  $^{29}\text{Si}$  NMR was performed by a Bruker DSX-400WB, Germany. The samples were treated at 180 °C for 2 h and then ground into fine powder. The thermal degradation of composite was examined using a thermogravimetric analyzer (TGA) (Perkin Elmer TGA 7) from room temperature to 800 °C at a rate of 10 °C/min under an atmosphere of nitrogen. The measurements were made on 6–10 mg samples. Weight-loss/temperature curves were plotted.

## 3. Results and Discussion

### 3.1. Characterization of Si-PU/APTS-GPTS Hybrid

The PDMS with –OH functional groups was used for a modification reaction with epoxy, and FTIR was used for structural characterization. Figure 1 shows the FTIR spectra of the PDMS with –OH, epoxy, and FPDMS, revealing that the PDMS had a large characteristic absorption peak of –OH at 3600–3200  $\text{cm}^{-1}$  [11,12] and an Si–O–Si functional group at 1080  $\text{cm}^{-1}$  [13]. The epoxy also exhibited a large oxirane ring at 910  $\text{cm}^{-1}$  [14,15]. FPDMS was formed after a ring opening reaction. In the spectra, we observed the disappearance of the oxirane ring and the appearance of a C–O characteristic absorption peak at 1107  $\text{cm}^{-1}$  [16]. These results reveal that the ring opening reaction was successful.

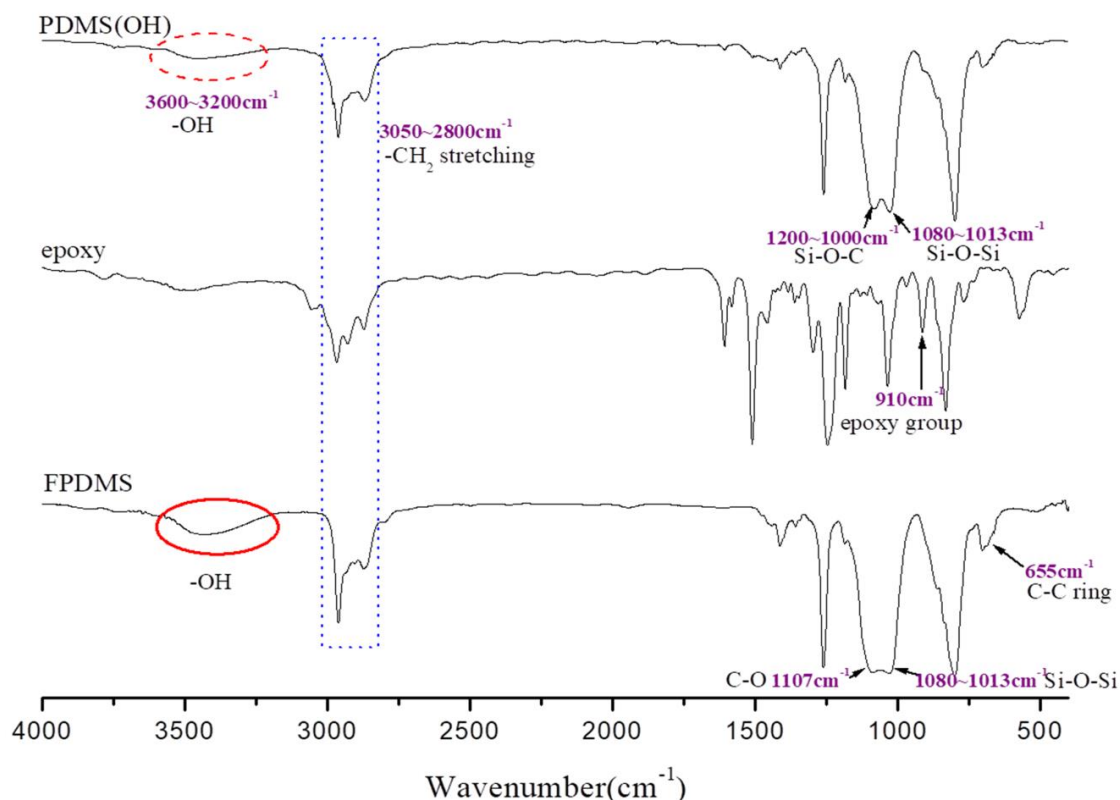


Figure 1. FTIR spectra of PDMS(OH), epoxy and FPDMS.

Figure 2 shows the FTIR spectra of the prepolymer that was generated from the reaction between IPDI and FPDMS. In Figure 2, the  $\text{-NCO}$  functional group of IPDI was clearly observed at  $2270\text{ cm}^{-1}$  [17], and the  $\text{-OH}$  functional group of FPDMS was observed at  $3600\text{--}3200\text{ cm}^{-1}$  [11,12]; the two reacted to produce a prepolymer. The spectra revealed that the characteristic absorption peak of  $\text{-NCO}$  partially disappeared, and the remaining  $\text{-NCO}$  functional groups were beneficial to the next stage of the reaction. Additionally, the reaction between IPDI and FPDMS resulted in the appearance of characteristic absorption peaks of  $\text{-NH}$  at  $3320\text{ cm}^{-1}$  [18],  $\text{C-N}$  at  $1310\text{ cm}^{-1}$  [19], and  $\text{C=O}$  at  $1700\text{--}1630\text{ cm}^{-1}$  [20]. These results confirm that the IPDI–FPDMS reaction had occurred.

As shown in Figure 3, the characteristic absorption peak of  $\text{CH}_2$  stretching on the APTS spectrum appeared at  $3050\text{--}2800\text{ cm}^{-1}$  [16,21], and those of  $\text{N-H}$ ,  $\text{Si-O-C}$ , and  $\text{Si-OEt}$  were at  $1640\text{--}1550\text{ cm}^{-1}$  [22,23],  $1200\text{--}1000\text{ cm}^{-1}$  [24], and  $1180\text{ cm}^{-1}$  [25], respectively. Moreover, the characteristic absorption peak of the oxirane ring group on the GPTS spectrum was at  $910\text{ cm}^{-1}$  [14,15]. After the ring opening reaction between APTS and GPTS, the spectra clearly showed the disappearance of the oxirane ring and the appearance of a  $\text{C-N}$  characteristic absorption peak at  $1310\text{ cm}^{-1}$  [19], revealing that APTS–GPTS underwent a successful ring opening reaction. Moreover, the APTS–GPTS spectrum retained the characteristic absorption peaks originally on the APTS and GPTS spectra, also confirming the success of the reaction.

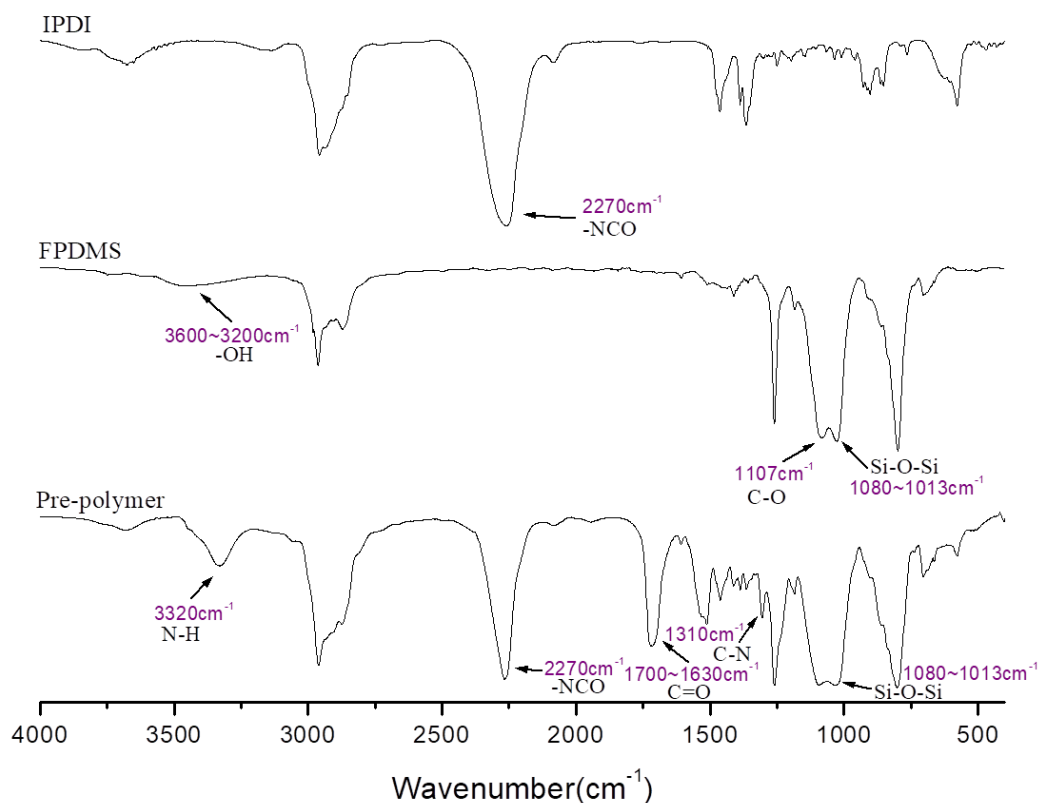


Figure 2. FTIR spectra of IPDI, FPDMS and prepolymer.

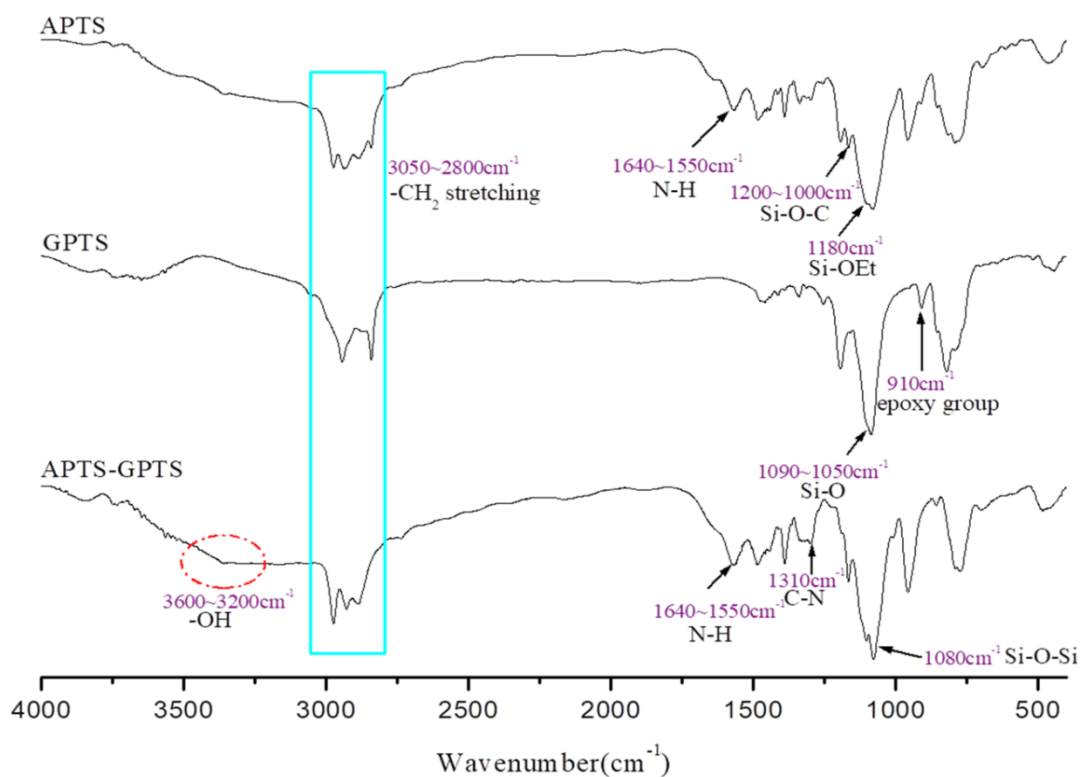
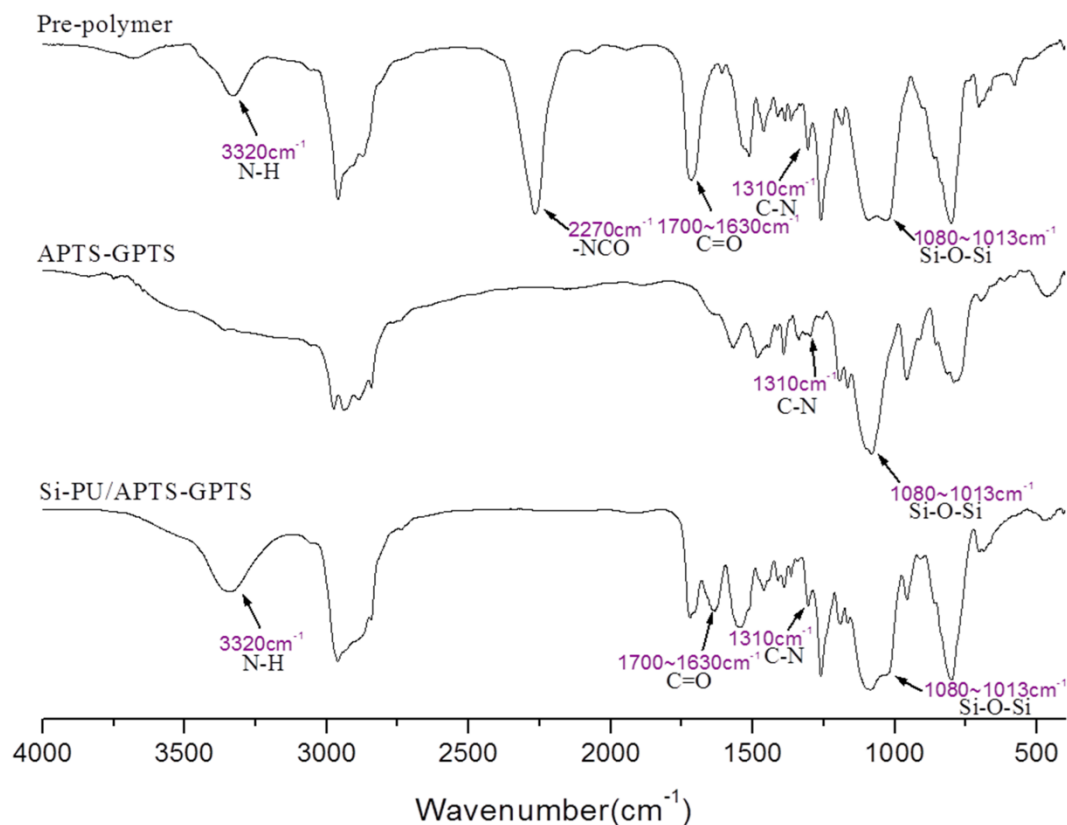


Figure 3. FTIR spectra of APTS, GPTS and APTS-GPTS.

Figure 4 shows that the -NCO functional group of the prepolymer at  $2270\text{ cm}^{-1}$  [17] and the -OH functional group of APTS-GPTS at  $3600\text{--}3200\text{ cm}^{-1}$  [11,12] reacted. Because the -NCO functional group fully reacted with the -OH functional group, the -NCO functional group on the

Si-PU/APTS-GPTS spectrum disappeared and the N-H characteristic absorption peak became more evident at  $3320\text{ cm}^{-1}$  [18]; other functional groups originally on the prepolymer and APTS-GPTS spectra were also present. This demonstrated that the Si-PU/APTS-GPTS hybrid material had been successfully fabricated.



**Figure 4.** FTIR spectra of pre-polymer, APTS-GPTS and Si-PU/APTS-GPTS.

### 3.2. Network Structure of Si-PU/APTS-GPTS Hybrid

Solid-state  $^{29}\text{Si}$  NMR spectroscopy can provide valuable and accurate information on the siloxane structure. Solid-state  $^{29}\text{Si}$  NMR spectroscopy was used to identify the structure of Si-PU/APTS-GPTS after it underwent the synthesis reaction. During the synthesis reaction, sol-gel technology was used to observe the hydrolysis- condensation level of the material. Because three trialkoxy groups (T) existed at one end of the APTS and GPTS, the structure of the APTS and GPTS was T-shaped. On the other end, the organic chain  $\text{NH}_2$  and epoxy underwent a ring opening reaction. The T group end of the APTS and GPTS further underwent hydrolysis-condensation to form a Si-O-Si network structure that displayed high stability. Based on the level of hydrolysis-condensation, the absorption peak of the mono-substituted T was at  $-45\sim-48\text{ ppm}$  and was defined as the  $\text{T}^1$  structure [26,27], the absorption peak of di-substituted T was at  $-56\sim-62\text{ ppm}$  and was defined as the  $\text{T}^2$  structure [26,28], and the absorption peak of tri-substituted T was at  $-66$  to  $-69\text{ ppm}$  and was defined as the  $\text{T}^3$  structure [26,27].

Figure 5 shows the solid-state  $^{29}\text{Si}$  NMR spectrum of Si-PU/APTS-GPTS hybrid material. As shown, the structure of Si-PU/APTS-GPTS consisted of T-shaped structures, with the  $\text{T}^3$  structure being the primary structure. Through peak separation, the integral areas of the  $\text{T}^1$ ,  $\text{T}^2$ , and  $\text{T}^3$  structures were obtained. Accordingly, the structure of the siloxane composite comprised 20.1% of the  $\text{T}^1$  structure, 34.1% of the  $\text{T}^2$  structure, and 46.0% of the  $\text{T}^3$  structure. Subsequently, the condensation density ( $\text{Dc}\%$ ) of Si-PU/APTS-GPTS was calculated as 75.4% using Equation (1) [29]. The high  $\text{Dc}\%$  indicated a compact network structure in the material, that the Si-O-Si bonds had formed a favorable network

structure, and that the Si-O bond possessed high bond energy. This could effectively enhance the thermal stability of the hybrid material. The results are shown in Table 1.

$$Dc(\%) = \frac{1 \times (\%areaT^1) + 2 \times (\%areaT^2) + 3 \times (\%areaT^3)}{3} \tag{1}$$

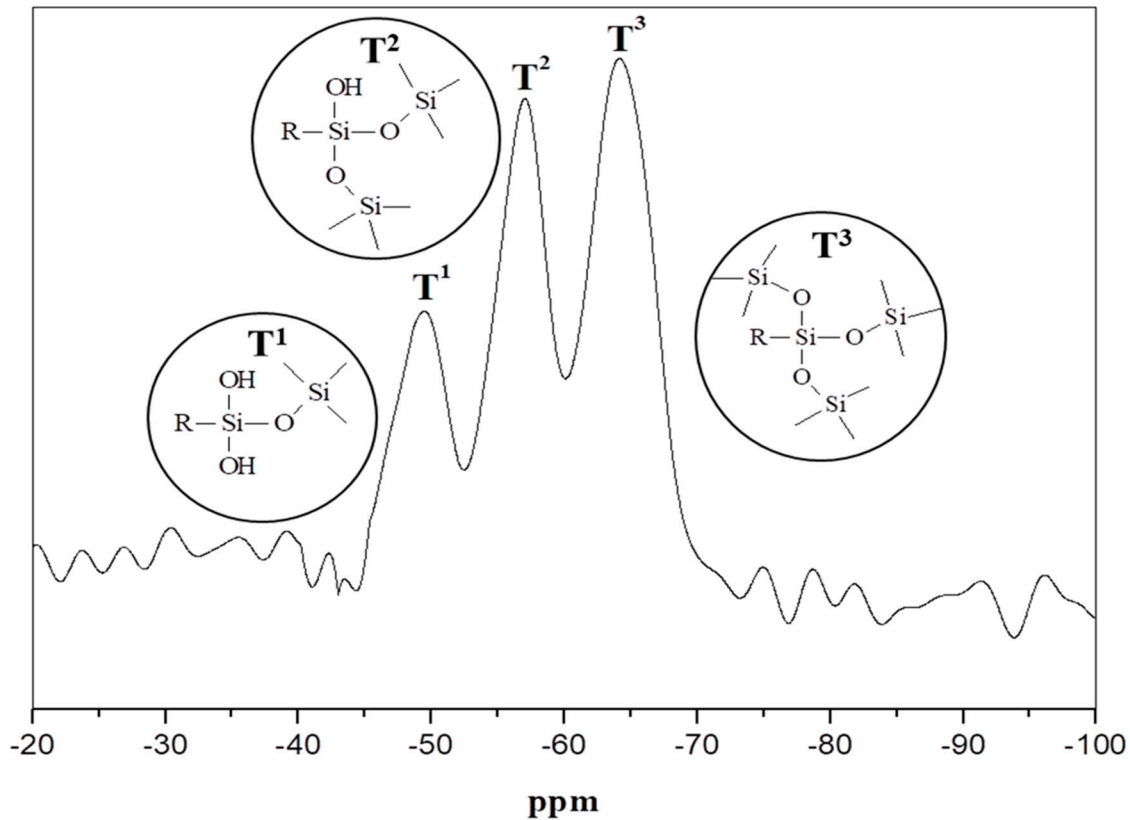


Figure 5. Solid-state <sup>29</sup>Si NMR spectra of Si-PU/APTS-GPTS.

Table 1. Distribution of area proportion.

Sample NO.	Area (%)			Dc (%)
	T <sup>1</sup>	T <sup>2</sup>	T <sup>3</sup>	
Si-PU/APTS-GPTS	20.1	34.1	46.0	75.4

### 3.3. Thermogravimetric Analysis

Based on the microbalance principle, a thermogravimetric analyzer records the weight loss of samples according to changes in the physical and chemical properties of substances as the temperature and time increase, thereby determining the thermal stability of materials. In the TGA, the heating rate was set to 20 °C/min and was measured in a nitrogen atmosphere. When APTS-GPTS was added to Si-PU at different contents, the weight loss changed as the temperature increased. The results are shown in Figures 6 and 7 and Table 2.

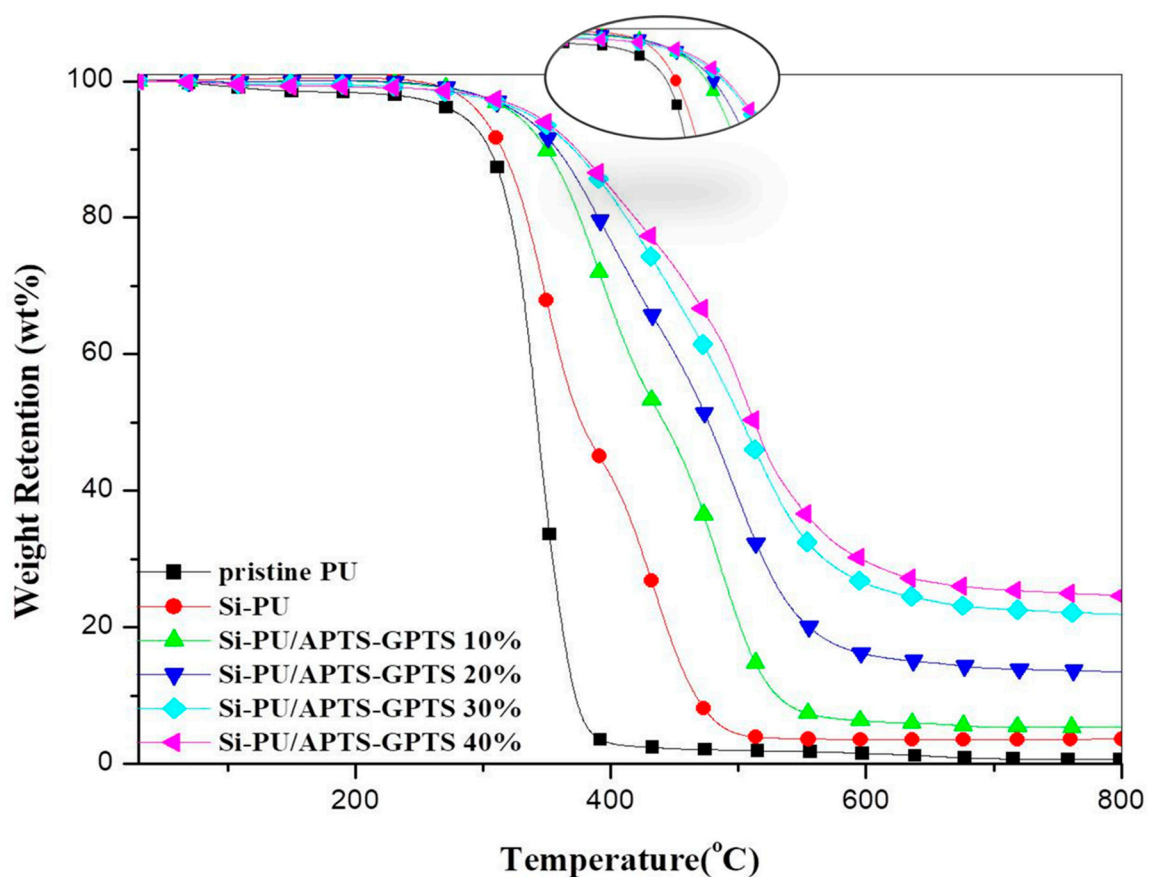


Figure 6. TGA curves of Pristine PU and Si-PU/APTS-GPTS composites in N<sub>2</sub>.

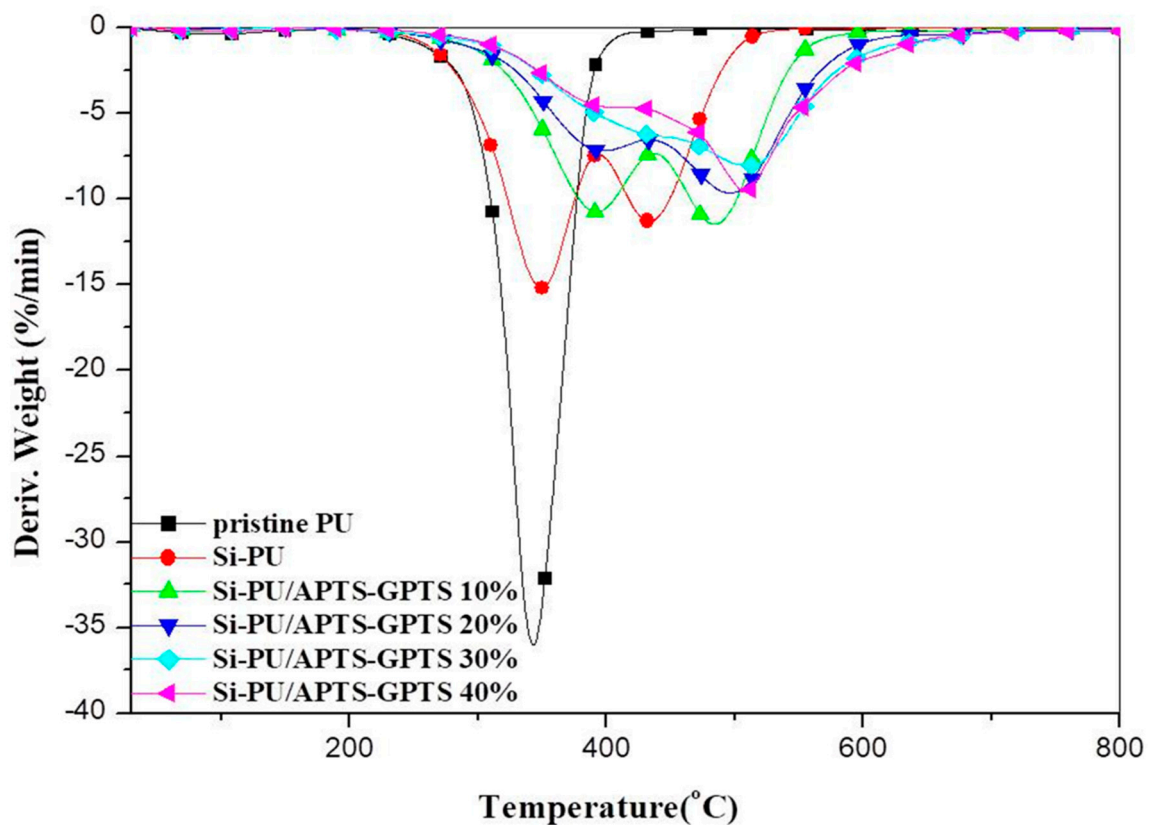


Figure 7. Derivative curves of pristine PU and Si-PU/APTS-GPTS composites in N<sub>2</sub>.

**Table 2.** Thermal properties of pristine PU and Si-PU/APTS-GPTS composites.

Sample NO.	<sup>a</sup> T <sub>d5</sub> (°C)	<sup>b</sup> T <sub>max</sub> (°C)		<sup>c</sup> R <sub>max</sub> (wt%/min)		IPDT (°C)	C.Y (wt %)
		1st	2nd	1st	2nd		
Pristine PU	273	343	-	-36.0	-	348	0.7
Si-PU	294	349	434	-15.2	-11.3	430	3.7
Si-PU/APTS-GPTS 10%	318	392	484	-10.7	-11.5	509	5.3
Si-PU/APTS-GPTS 20%	321	397	496	-7.2	-9.6	641	13.5
Si-PU/APTS-GPTS 30%	326	510	-	-8.0	-	794	21.9
Si-PU/APTS-GPTS 40%	330	404	508	-4.6	-9.6	859	24.7

<sup>a</sup> T<sub>d5</sub> is the temperature when the weight loss of sample reaches its 5%. <sup>b</sup> T<sub>max</sub> corresponds to the temperature of maximum degradation rate. <sup>c</sup> R<sub>max</sub> corresponds to the maximum thermal degradation rate.

Figure 6 and Table 2 show the changes in the decomposition curves. The temperature (T<sub>d5</sub>) of pristine PU was 273 °C when the weight loss was 5%. After APTS-GPTS was added to Si-PU, and as the concentration of APTS-GPTS increased, T<sub>d5</sub> increased considerably to 330 °C (Si-PU/APTS-GPTS 40% composite) when the weight loss of the hybrid material was 5%. As the concentration of APTS-GPTS increased, the char yield increased, particularly at 800 °C. The char yield increased from 0.7 wt% for pristine PU to 24.7 wt% for the Si-PU/APTS-GPTS 40% composite. This can be attributed to the surface migration of Si in the APTS-GPTS structure when APTS-GPTS underwent thermal decomposition [30,31]. The surface migration generated a compact SiO<sub>2</sub> structure to protect the internal part of the material. The benzene ring contributed to the char yield; therefore, the char layer featured oxidation resistance to prevent combustion. Figure 6 shows the large differences in weight retention between different samples, revealing that APTS-GPTS increased the thermal stability of Si-PU.

The derivative thermogravimetric curves are displayed in Figure 7. As shown, as the temperature changed, the temperature of maximum degradation rate of pristine PU was 343 °C. As the concentration of APTS-GPTS increased, the temperature of maximum degradation rate increased to 508 °C (Si-PU/APTS-GPTS 40%). Moreover, maximum degradation rate for pristine PU was -36 wt %/min. After adding APTS-GPTS, it effectively slowed down to -9.6 wt%/min and greatly slowed down the rate of thermal degradation. The above proved that the addition of APTS-GPTS nanoparticles could effectively improve the thermal stability of hybrid materials.

#### 3.4. Integral Procedural Decomposition Temperature (IPDT)

The TGA data were used to plot a diagram as Figure 8. The area under the decomposition curve was obtained through integration in following picture, and was then substituted into Equation (2) to calculate the IPDT, which was used to evaluate the thermal stability of the composite materials [32]. The two major factors that influenced the calculation results were the initial decomposition temperature and char yield. High values for these two factors indicated favorable thermal stability, heat resistance, and IPDT, whereas low IPDT indicated poor overall thermal stability of the materials.

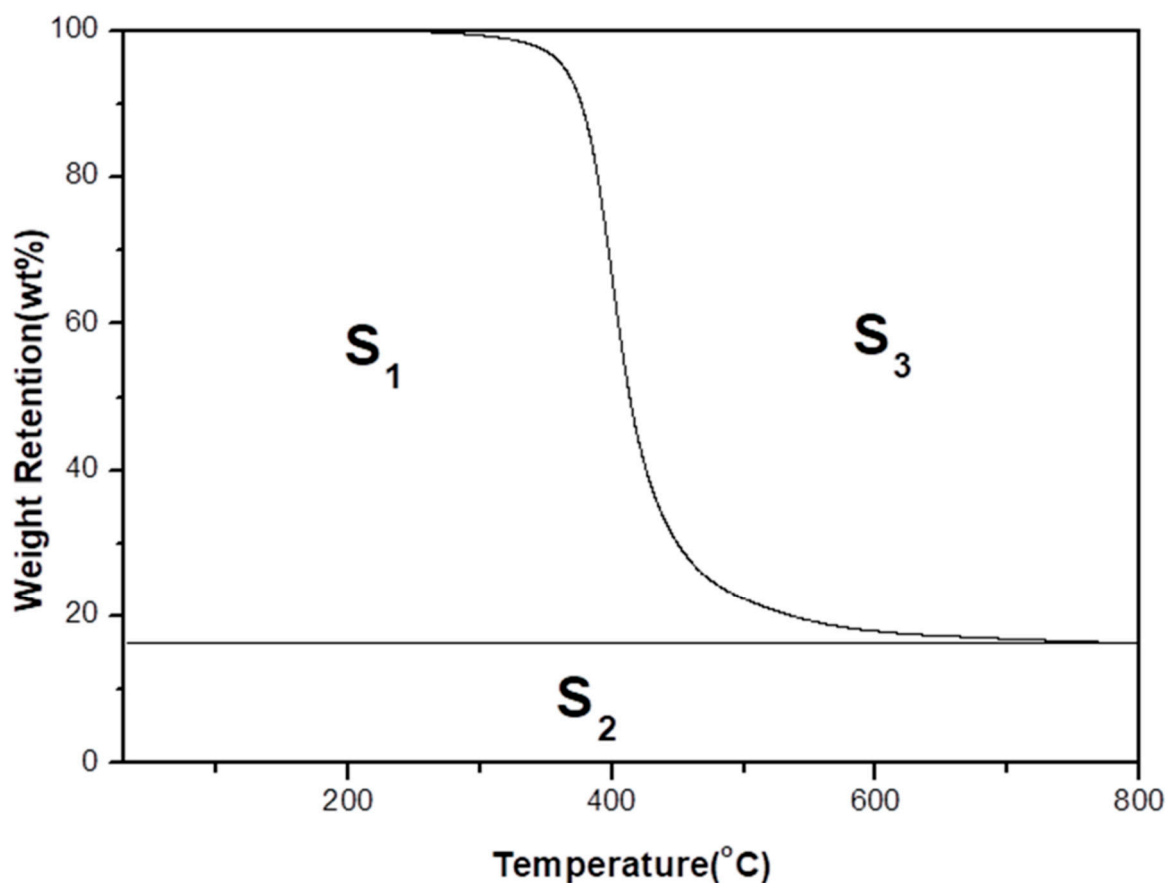


Figure 8. TGA plot.

The calculation was performed using the following equation:

$$A^* = (S_1 + S_2)/(S_1 + S_2 + S_3)$$

$$K^* = (S_1 + S_2)/S_1$$

where  $T_i$  is the initial experimental temperature, and  $T_f$  is the final experimental temperature. The IPDT can be obtained by incorporating the calculated values of  $T_i$ ,  $T_f$ ,  $S_1$ ,  $S_2$ , and  $S_3$  into the Equation (2).

$$\text{IPDT } (^\circ\text{C}) = A^* \times K^* \times (T_f - T_i) + T_i \quad (2)$$

Figure 9 and Table 2 show that the IPDT of pristine PU was 348 °C, which increased to 859 °C after APTS-GPTS was added to 40%; that is, the IPDT of the hybrid material was greater than that of the pristine PU by 511 °C, and the thermal stability substantially increased by approximately 247%. These results demonstrate that adding APTS-GPTS enhanced the thermal stability of PU hybrid materials, and such high thermal stability could be attributed to the superior degradation resistance of APTS-GPTS at high temperature.

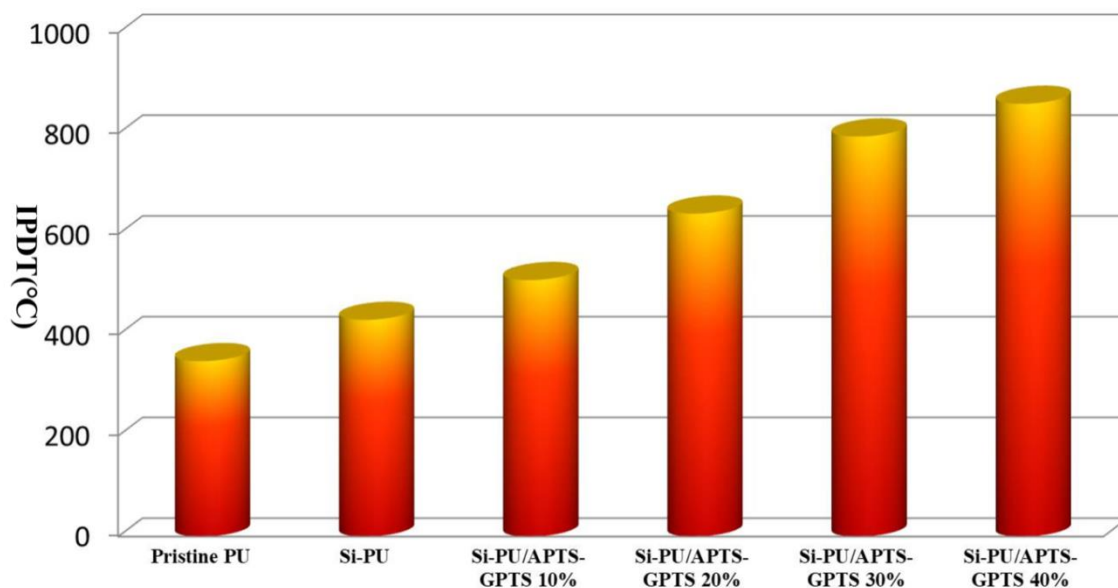


Figure 9. The IPDT data of pristine PU and Si-PU/APTS-GPTS composites.

### 3.5. Experimental and Calculated Data

Based on the substitution of the TGA curves, calculated data were obtained using Equation (3). The calculated data were then compared with the experimental data to understand whether the data exhibited a positive deviation when APTS-GPTS was added to polymer materials. A positive deviation denoted a favorable interaction between the organic and inorganic phase. The equations for the calculated data are as follows [33]:

$$\text{Calculated data 10\%} = \text{Si-PU} \cdot 90\% + \text{APTS-GPTS} \cdot 10\%$$

$$\text{Calculated data 20\%} = \text{Si-PU} \cdot 80\% + \text{APTS-GPTS} \cdot 20\%$$

$$\text{Calculated data 30\%} = \text{Si-PU} \cdot 70\% + \text{APTS-GPTS} \cdot 30\%$$

$$\text{Calculated data 40\%} = \text{Si-PU} \cdot 60\% + \text{APTS-GPTS} \cdot 40\%$$

The difference between the experimental and calculated TGA curves revealed a strong interaction between the inorganic phase of APTS-GPTS and the organic phase of Si-PU (Figure 10). The TGA curve of the Si-PU/APTS-GPTS 40% composite showed a char yield higher than that of the calculated TGA curve by 8.3%, demonstrating that the experiment data in this study produced satisfactory thermal stability [34].

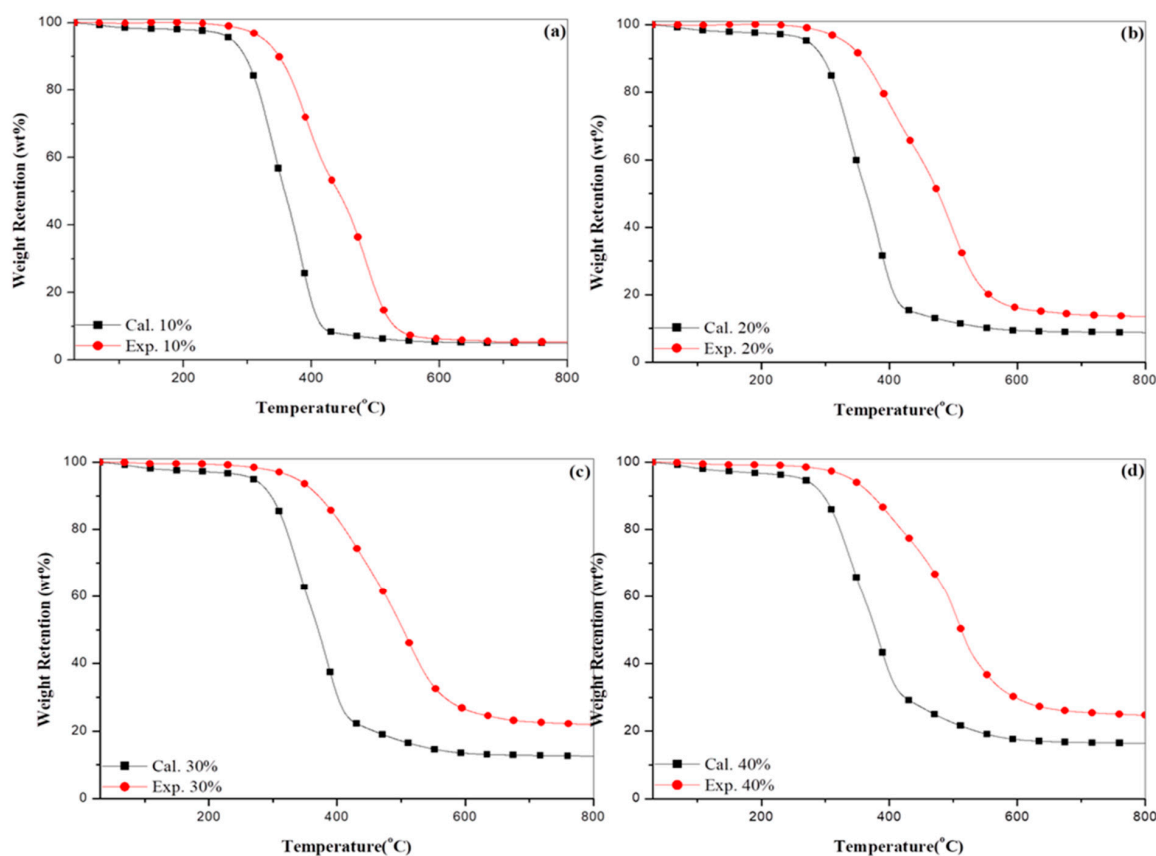


**Figure 10.** Comparison of calculated and experimental TGA curves for: (a) Si-PU/APTS-GPTS 10%; (b) Si-PU/APTS-GPTS 20%; (c) Si-PU/APTS-GPTS 30%; and (d) Si-PU/APTS-GPTS 40% composites.

Changes in the initial decomposition temperature and char yield were examined, as shown in Table 3. The experimental decomposition temperature ( $T_{d5}$ ) of the Si-PU/APTS-GPTS 40% composite was higher than the calculated temperature by 88 °C [34]. The initial decomposition temperatures for the four samples were considerably higher than the calculated temperatures. Furthermore, the char yields of experimental data all exhibited a positive deviation. These results reveal that the combination of organic and inorganic phases effectively increased the initial decomposition temperature and the char yield. Therefore, the satisfactory results were not the effect of a single material, but represented a synergistic effect of all the materials in the composite.

**Table 3.** Comparison of calculated and experimental TGA data of Si-PU/APTS-GPTS composites.

Sample NO.	Cal.		Exp.	
	Td5	C.Y. (wt%) at 800 °C	Td5	C.Y. (wt%) at 800 °C
Si-PU/APTS-GPTS 10%	268	5.0	318	5.3
Si-PU/APTS-GPTS 20%	263	8.8	321	13.5
Si-PU/APTS-GPTS 30%	256	12.6	326	21.9
Si-PU/APTS-GPTS 40%	242	16.4	330	24.7

#### 4. Conclusions

This study conducted the structural identification of hybrid materials synthesized with APTS-GPTS by using FTIR and  $^{29}\text{Si}$  NMR. The identification verified that introducing APTS-GPTS to the polymer materials successfully prepared the Si-PU/APTS-GPTS hybrid materials. Regarding the thermal properties, this study revealed that adding siloxane to siloxane-PU effectively enhanced thermal stability and heat resistance. The thermal stability was then measured using IPDT, and the results show

that the thermal stability of the materials increased considerably. The experimental and calculated data exhibit a positive deviation, demonstrating that APTS-GPTS interacted with the polymer materials. The results of this study reveal that APTS-GPTS effectively improved the thermal stability of PU.

**Author Contributions:** Conceptualization, C.-L.C.; Methodology, S.-H.L.; Software, M.-Y.S.; Validation, C.-F.K., H.-C.K. and C.-L.C.; Formal Analysis, C.-L.C.; Investigation, C.-Y.K.; Data Curation, C.-L.C.; Writing-Original Draft Preparation, C.-L.C.; Writing-Review & Editing, S.-H.L.; Visualization, S.-H.L.

**Funding:** This research was funded by National Science Council of the Republic of China grant MOST-105-2221-E-241-001-MY3.

**Acknowledgments:** The authors would like to express their appreciation to the National Science Council of the Republic of China for financial support of this study under grant MOST-105-2221-E-241-001-MY3.

**Conflicts of Interest:** The authors declare no conflict of interest.

## References

1. Kumar, R.; Yadav, R.; Kolhe, M.A.; Bhosale, R.S.; Narayan, R. 8-Hydroxypyrene-1,3,6-trisulfonic acid trisodium salt (HPTS) based high fluorescent, pH stimuli waterborne polyurethane coatings. *Polymer* **2018**, *136*, 157–165. [[CrossRef](#)]
2. Bedő, D.; Imre, B.; Domján, A.; Schöne, P.; Vancsoe, G.J.; Pukánszky, B. Coupling of poly(lactic acid) with a polyurethane elastomer by reactive processing. *Eur. Polym. J.* **2017**, *97*, 409–417. [[CrossRef](#)]
3. Bing, H.; Lin, Y. Highly heat-resistant silicon-containing polyurethane-imide copolymers: Synthesis and thermal mechanical stability. *Eur. Polym. J.* **2017**, *91*, 337–353.
4. Pagacz, J.; Hebdab, E.; Janowski, B.; Sternik, D.; Janciab, M.; Pielichowski, K. Thermal decomposition studies on polyurethane elastomers reinforced with polyhedral silsesquioxanes by evolved gas analysis. *Polym. Degrad. Stabil.* **2018**, *149*, 129–142. [[CrossRef](#)]
5. Chen, J.; Zhang, J.; Zhu, T.; Hua, Z.; Chen, Q.; Yu, X. Blends of thermoplastic polyurethane and polyether-polyimide: preparation and properties. *Polymer* **2001**, *42*, 1493–1500. [[CrossRef](#)]
6. Voronkov, A.V.; Kopylov, V.M.; Parsons, I.W. Furan-containing modified organosilicon polymers: Preparation, properties and some applications. *Eur. Polym. J.* **1997**, *7*, 979–990. [[CrossRef](#)]
7. Macan, J. Thermal degradation of epoxy-silica organic-inorganic hybrid materials. *Polym. Degrad. Stabil.* **2006**, *91*, 122–127. [[CrossRef](#)]
8. Heidsieck, S.U.H.; Dörrich, S.; Weidner, R.; Rieger, B. Branched siloxanes as possible new heat transfer fluids for application in parabolic through solar thermal power plants. *Sol. Energy Mater. Sol. Cells* **2017**, *161*, 278–284. [[CrossRef](#)]
9. Zhao, Z.; Jin, Q.; Zhang, N.; Guo, X.; Yan, H. Preparation of a novel polysiloxane and its synergistic effect with ammonium polyphosphate on the flame retardancy of polypropylene. *Polym. Degrad. Stabil.* **2018**, *150*, 73–85. [[CrossRef](#)]
10. Chiang, C.L.; Chang, R.C. Synthesis, characterization, and thermal properties of bridged polysilsesquioxanes-molecular nanocomposites. In Proceedings of the 13th European Conference on Composite Materials (ECCM 2008), Stockholm, Sweden, 2–5 June 2008.
11. Kusumoto, T.; Mori, Y.; Kanasaki, M.; Ueno, T.; Kameda, Y.; Oda, K.; Kodaira, S.; Kitamura, H.; Barillon, R.; Yamauchi, T. Yields on the formation of OH groups and the loss of CH groups along nuclear tracks in PADC films. *Radiat. Meas.* **2015**, *83*, 59–62. [[CrossRef](#)]
12. Sritham, E.; Gunasekaran, S. FTIR spectroscopic evaluation of sucrose-maltodextrin-sodium citrate bioglass. *Food Hydrocoll.* **2017**, *70*, 371–382. [[CrossRef](#)]
13. Kim, J.; Jung, D.; Park, Y.; Kim, Y.; Moon, D.W.; Lee, T.G. Quantitative analysis of surface amine groups on plasma-polymerized ethylenediamine films using UV-visible spectroscopy compared to chemical derivatization with FT-IR spectroscopy, XPS and TOF-SIMS. *Appl. Surf. Sci.* **2007**, *253*, 4112–4118. [[CrossRef](#)]
14. Sideridou, I.D.; Vouvoudi, E.C.; Papadopoulos, G.D. Epoxy polymer Hxtal NYL-1TM used in restoration and conservation: Irradiation with short and long wavelengths and study of photo-oxidation by FT-IR spectroscopy. *J. Cult. Herit.* **2016**, *18*, 279–289. [[CrossRef](#)]
15. Bagherzadeh, M.R.; Daneshvar, A.; Shariatpanahi, H. Novel water-based nanosiloxane epoxy coating for corrosion protection of carbon steel. *Surf. Coat. Technol.* **2012**, *206*, 2057–2063. [[CrossRef](#)]

16. Colombani, J.; Chauvet, E.; Amat, S.; Dupuy, N.; Gigmes, D. A FTIR/chemometrics approach to characterize the gamma radiation effects on iodine/epoxy-paint interactions in Nuclear Power Plants. *Anal. Chim. Acta* **2017**, *960*, 53–62. [[CrossRef](#)] [[PubMed](#)]
17. Gallego, R.; Arteaga, J.F.; Valencia, C.; Franco, J.M. Thickening properties of several NCO-functionalized cellulose derivatives in castor oil. *Chem. Eng. Sci.* **2015**, *134*, 260–268. [[CrossRef](#)]
18. Mishra, A.K.; Narayan, R.; Raju, K.V.S.N.; Aminabhavi, T.M. Hyperbranched polyurethane (HBPU)-urea and HBPU-imide coatings: Effect of chain extender and NCO/OH ratio on their properties. *Prog. Org. Coat.* **2012**, *74*, 134–141. [[CrossRef](#)]
19. Sheikh, Z.; Khan, A.S.; Roohpour, N.; Glogauer, M.; Rehman, I.u. Protein adsorption capability on polyurethane and modified-polyurethane membrane for periodontal guided tissue regeneration applications. *Mater. Sci. Eng. C* **2016**, *68*, 267–275. [[CrossRef](#)] [[PubMed](#)]
20. Zhou, H.; Wang, H.; Tian, X.; Zheng, K.; Cheng, Q. Effect of 3-Aminopropyltriethoxysilane on polycarbonate based waterborne polyurethane transparent coatings. *Prog. Org. Coat.* **2014**, *77*, 1073–1078. [[CrossRef](#)]
21. Mahdavi, M.; Ahmad, M.B.; Haron, M.J.; Gharayebi, Y.; Shameli, K.; Nadi, B. Fabrication and characterization of SiO<sub>2</sub>/(3-aminopropyl) triethoxysilane coated magnetite nanoparticles for lead (II) removal from aqueous solution. *J. Inorg. Organomet. Polym.* **2013**, *23*, 599–607. [[CrossRef](#)]
22. Pontón, P.I.; d’Almeida, J.R.M.; Marinkovic, B.A.; Savić, S.M.; Mancic, L.; Rey, N.A.; Morgado, E., Jr.; Rizzo, F.C. The effects of the chemical composition of titanate nanotubes and solvent type on 3-aminopropyltriethoxysilane grafting efficiency. *Appl. Surf. Sci.* **2014**, *301*, 315–322. [[CrossRef](#)]
23. Ramírez, C.; Rico, M.; Torres, A.; Barral, L.; López, J.; Montero, B. Epoxy/POSS organic–inorganic hybrids: ATR-FTIR and DSC studies. *Eur. Polym. J.* **2008**, *44*, 3035–3045. [[CrossRef](#)]
24. Jain, S.; Goossens, H.; Picchioni, F.; Magusin, P.; Mezari, B.; van Duin, M. Synthetic aspects and characterization of polypropylene–silica nanocomposites prepared via solid-state modification and sol–gel reactions. *Polymer* **2005**, *46*, 6666–6681. [[CrossRef](#)]
25. Han, Y.H.; Taylor, A.; Mantle, M.D.; Knowles, K.M. Sol–gel-derived organic–inorganic hybrid materials. *J. Non-Cryst. Solids* **2007**, *353*, 313–320. [[CrossRef](#)]
26. Fan, Y.; Wang, G.; Huang, X.; Bu, J.; Sun, X.; Jiang, P. Molecular structures of (3-aminopropyl)trialkoxysilane on hydroxylated barium titanate nanoparticle surfaces induced by different solvents and their effect on electrical properties of barium titanate based polymer nanocomposites. *Appl. Surf. Sci.* **2016**, *364*, 798–807.
27. Jin, Q.F.; Liao, G.X.; Jian, X.G. Synthesis and characterization of trimethoxysilyl-functionalized poly(phthalazinone ether ketone). *Chin. Chem. Lett.* **2007**, *8*, 1137–1140. [[CrossRef](#)]
28. Paquet, O.; Brochier Salon, M.C.; Zeno, E.; Belgacem, M.N. Hydrolysis-condensation kinetics of 3-(2-amino-ethylamino)propyl-trimethoxysilane. *Mater. Sci. Eng. C* **2012**, *32*, 487–493. [[CrossRef](#)]
29. Shea, K.J.; Loy, D.A.; Webster, O. Arylsilsesquioxane Gels and Related Materials. New Hybrids of Organic and Inorganic Networks. *J. Am. Chem. Soc.* **1992**, *114*, 6700–6710. [[CrossRef](#)]
30. Shi, Y.; Wang, G. The novel silicon-containing epoxy/PEPA phosphate flame retardant for transparent intumescent fire resistant coating. *Appl. Surf. Sci.* **2016**, *385*, 453–463. [[CrossRef](#)]
31. Wu, C.S.; Liu, Y.L.; Chiu, Y.S. Epoxy resins possessing flame retardant elements from silicon incorporated epoxy compounds cured with phosphorus or nitrogen containing curing agents. *Polymer* **2002**, *43*, 4277–4284. [[CrossRef](#)]
32. Qian, Y.; Wei, P.; Jiang, P.; Zhao, X.; Yu, H. Synthesis of a novel hybrid synergistic flame retardant and its application in PP/IFR. *Polym. Degrad. Stabil. P* **2011**, *96*, 1134–1140. [[CrossRef](#)]
33. Gao, F.; Tong, L.; Fang, Z. Effect of a novel phosphorous–nitrogen containing intumescent flame retardant on the fire retardancy and the thermal behaviour of poly(butylene terephthalate). *Polym. Degrad. Stabil.* **2006**, *91*, 1295–1299. [[CrossRef](#)]
34. Jakic, M.; Vrandecic, N.S.; Klari, I. Thermal degradation of poly(vinyl chloride)/poly(ethylene oxide) blends: Thermogravimetric analysis. *Polym. Degrad. Stabil.* **2013**, *98*, 1738–1743. [[CrossRef](#)]

